arXiv:cond-mat/0109473v1 [cond-mat.soft] 25 Sep 2001

Effect of Director Distortions on Polymer-Liquid Crystal Phase Separation

D. Voloschenko, O. P. Pishnyak, S. V. Shiyanovskii, and O. D. Lavrentovich
Chemical Physics Interdisciplinary Program and Liquid Crystal Institute, Kent State University, Kent, OH 44242, USA
(February 1, 2008)

Abstract

We study photopolymerization in a low-molecular weight liquid crystal with non-uniform director gradients. Phase separation results in spatially non-uniform distribution of polymer density controlled by the distorted nematic matrix. Director-gradient-controlled polymerization provides a new and useful technique to assemble micron-scale polymer architectures.

PACS number(s): 61.30.Gd, 64.75.+g

Typeset using REVTEX

Composites of polymers and liquid crystals (LCs) are subject of intensive studies for electrooptical applications [1]. The most popular method to produce composites such as polymer-dispersed LCs (PDLCs) and polymer-stabilized LCs (PSLCs) is ptotoinduced phase separation in a mixture of a non-reactive LC and a reactive monomer. Morphology of the product depends on many factors, such as solubility [2], diffusivity [3], concentration [4] and reactivity of components, spatial distribution of light intensity [5], electric field gradients [6], time scales of polymerization [7–9], etc. Phase separation from the LC continuous state is of especial interest, as the morphology can be influenced by the orientational order of the LC solvent. For example [10], phase-separating droplets of isotropic fluid form chains parallel to the director $\hat{\mathbf{n}}$, which specifies the average orientation of LC molecules. In PSLCs, polymer strands can align along $\hat{\mathbf{n}}$, especially when formed from a mesogenic monomer [1,11]. However, it is not clear how the morphology would be altered if $\hat{\mathbf{n}}$ is distorted and these distortions are non-uniform in space. Experiments on periodically-distorted cholesteric gratings demonstrate that the phase-separating component has density modulation with the period set by the modulated $\hat{\mathbf{n}}$ [12,13]. There are at least three possible mechanisms of this effect. (1) Since the LC is an elastic medium, the phase separating component might be forced to accumulate in the sites with the highest energy of director distortions, especially when this component forms compact particles rather than fibrils. (2) Polymer density might vary because of spatial changes of the angle between light polarization $\mathbf{P}$ and $\hat{\mathbf{n}}$. (3) Variations in light intensity caused by 'lens' effects in the distorted birefringent LC.

In this work, we separate the three mechanisms and demonstrate that spatial variation of the director gradients can indeed lock-in the spatial distribution of the precipitating component.

We use the nematic E7 (EM Industries) with a small (≈5wt%) amount of the UV-curable prepolymer NOA65 comprised of trimethylol-propane diallyl ether, trimethylol-propane tris(thiol), isophorone diisocyanate ester, premixed with a benzophenone photoinitiator [14]. Photopolymerization proceeds by cross-linking reactions and results in compact morphologies with a reduced interfacial area between NOA65 and LC domains; LC is expelled from the polymerized NOA65 [6,8,9,15–18]. The latter feature makes NOA65 attractive for PDLCs in which LC droplets are well separated by the polymer matrix. Because of a small concentration of NOA65, our system is an "reverse" of PDLCs. The non-cured mixture preserves the nematic state at room temperature and upon heating to 53 C^0 [15]. We used a narrow-band UV lamp (wavelength $\lambda = 366$ nm) and a Glan-Thompson prism to polarize UV light linearly; light intensity after the polarizer was $I \approx 30\ \mu W/cm^2$. Experiments were performed at room temperature for the cells of thickness $d = 20\ \mu$m. First, we show that the polymerization rate depends on the angle between $\mathbf{P}$ and $\hat{\mathbf{n}}$.

Light polarization mechanism. The plates of LC cells were treated for planar alignment (rubbed polyimide layers), $\hat{\mathbf{n}}$ =const. Photopolymerization was induced by UV light with $\mathbf{P} \perp \hat{\mathbf{n}}$ or $\mathbf{P} \| \hat{\mathbf{n}}$. Comparison of otherwise identical cells shows that polymerization is faster when $\mathbf{P} \| \hat{\mathbf{n}}$ (Fig.1). The first few hours of irradiation do not cure NOA65 completely: if irradiation is stopped and the sample is heated to 35-50 C^0, then the phase-separated NOA65-rich particles dissolve back into the nematic matrix. Note also that the NOA65 particles often form chains along the groves of rubbed polyimide; as discussed in Ref. [19], patterned substrates can influence the phase-separating morphologies.

Director inhomogeneity. To elucidate the role of director gradients on morphology

of phase-separation, we studied 90° twisted cells. The rubbing directions at the two plates of the cell are perpendicular to each other. The equally probable domains of opposite 90° twists, $(n_x, n_y, n_z) = (\cos \pi z/2d, \sin \pi z/2d, 0)$ and $(n_x, n_y, n_z) = (\cos \pi z/2d, -\sin \pi z/2d, 0)$ (the z axis is perpendicular to the cell plates), are separated by defects (disclinations [20]).

The cell configuration allows us to separate the lens and light polarization effects from the effect of director distortions, by chosing $\mathbf{P}||\hat{\mathbf{n}}$ at the plate of incidence, Fig.2,3. Since $d >> \lambda$, $\mathbf{P}$ rotates with $\hat{\mathbf{n}}$ remaining parallel to $\hat{\mathbf{n}}$ (Mauguin regime) within the twist domains. Therefore, the polarization effect facilitates polymerization within the twist domains but not at the domain boundary defect, where $\mathbf{P}$ is not parallel to $\hat{\mathbf{n}}$, because the Mauguin regime is violated [20]. Furthermore, light with $\mathbf{P}\|\hat{\mathbf{n}}$ propagates with a refractive index n_e, which is the maximum value of the refractive index in the optically positive E7; thus if the domain boundary acts as a lens, this lens can only be divergent. Therefore, both polarization and lens effects facilitate NOA65 precipitation within the domains but not at the domain boundaries.

In the experiment, the NOA65-rich particles start to appear everywhere, within the twist domains and at the domain boundaries. However, many particles that appear within the twist domains near the boundaries migrate toward the boundaries and are pinned there, Figs. 2,3. Smaller particles might coalesce into chains of big particles or even form continuous walls.

Qualitatively, the leading mechanism of aggregation in the regions with the highest LC distortions can be explained as follows. Initially, the nematic order is preserved in the whole specimen and the NOA65 monomers are distributed homogeneously [21]. A phase-separated NOA65 particle of a radius R_p eliminates the nematic order in the volume R_P^3. If $\hat{\mathbf{n}}$ were uniform, there would be no preferable site for the particle (we do not consider here the surface-mediated heterogeneous nucleation at the cell plates). However, in a distorted LC, elimination of the volume R_P^3 decreases the elastic energy by $E_V = KA^2R_P^3/\xi^2$, where K is the average elastic constant, A is the amplitude and ξ is the characteristic length of director distortions. The higher the distortions A/ξ, the higher the energy gain E_V of replacing the LC region with a particle.

There are other factors, such as director anchoring at the particle surface, which would act differently depending on whether R_p is smaller or larger than the length $L_p = K/W_p$, usually of the order of $(0.1 - 10)$ μm; W_p is the anchoring coefficient at the particle-nematic interface. When $R_p > L_p$, $\hat{\mathbf{n}}$ around the particle is determined mainly by the particle's surface propeties; the gain E_V might be larger or smaller than the energy E_{ind} of additional distortions induced around the particle. There are cases when $E_V > E_{ind}$ undoubtfully. For example, a spherical particle with perpendicular anchoring of $\hat{\mathbf{n}}$ placed in the LC with a radial director (point defect-hedgehog) would find the energy minimum at the center of the defect rather than in any other location, as clearly demonstrated for nematic colloids with water droplets [22]. It is, however, hard to find a universal description of E_{ind} and E_V when $R_p > L_p$. Fortunately, for $R_p < L_p$ (initial stages of polymerization), it is possible to show that the anchoring effects are not essential, and that E_V dominates to guide the particles toward the cites with the highest director gradients.

We use the standard free energy functional

$$F = \int\limits_V f\,(x,z)dV + \tfrac{1}{2}\int\limits_S W\left(1-(\hat{\nu}\cdot\hat{\mathbf{n}})^2\right)dS, \tag{1}$$

$$2f = K_1\left(div\hat{\mathbf{n}}\right)^2 + K_2\left(\hat{\mathbf{n}}\cdot curl\hat{\mathbf{n}}\right)^2 + K_3\left[\hat{\mathbf{n}}\times curl\hat{\mathbf{n}}\right]^2,$$

where K_1, K_2, and K_3 are the elastic constants of splay, twist, and bend, respectively; $\hat{\nu}$ is the normal to the polymer-liquid crystal interface. The change in the free energy caused by placing a polymer particle in a distorted LC is

$$\Delta E = -E_V + \Delta E_S + E_{ind}, \tag{2}$$

where $E_V = \int\limits_{V_P} f\,(x,z)\,dV_P$ is the elastic energy of the LC volume V_P that is excluded by the particle; ΔE_S is the difference in the anchoring energy at the surface S_P of the particle for homogeneous and distorted director fields; E_{ind} is the elastic energy of the additional distortions induced by the particle. For $R_p < L_p$,

$$E_V \cong \frac{1}{2}K\int\limits_{V_P}(\nabla\hat{\mathbf{n}})^2 dV_P \cong \frac{2}{3}\pi K\frac{R_p^3}{\xi^2}A^2 \tag{3}$$

dominates in Eq. (2), because $\Delta E_S = \frac{4\pi}{15}W_p R_P^4 div\left(\hat{\mathbf{n}}_0 div\hat{\mathbf{n}}_0 + \hat{\mathbf{n}}_0\times curl\hat{\mathbf{n}}_0\right) \cong \frac{4\pi W_p R_P^4 A^2}{15\xi^2}$ $\cong \frac{2R_P}{5L_P}E_V << E_V$ ($\hat{\mathbf{n}}_0$ is the director at the center of the LC region replaced by the particle) and, according to [23], $|E_{ind}| \cong \frac{W_p R_P}{5A^2K}\left|\Delta E_S\right| \leqslant |\Delta E_S|$. The tendency of particles to occupy the regions with high elastic free energy prevails over the entropy driven randomization if $|\Delta E| \approx E_V \geqslant k_B T$ and, therefore, $R_P \geqslant R_C = \sqrt[3]{\frac{k_B T\xi^2}{2KA^2}}$. For $K = 10^{-11}N$, $\xi = 5\mu m$, $A = 1$, and room temperature, one finds $R_C = 0.2\mu m$. To estimate time τ, required to drive the particle, one can use the Stokes formula for the drag force $F \cong \Delta E/\xi \cong 6\pi\alpha_4 R_P\bar{v}$, where α_4 is the Leslie viscosity coefficient and $\bar{v} \cong \xi/\tau$ is the average velocity of the particle. Substitution $|\Delta E| \approx E_V$ in the Stokes formula results in $\tau \approx \frac{9\alpha_4\xi^4}{KA^2R_P^2}$. For $\alpha_4 = 0.1$ Pa·s, $\xi = 5\mu m$, $R_P = 1\mu m$, and $A = 1$, the driving time $\tau \approx 50\ s$ is small enough to provide accumulation of NOA65-rich particles. However, its strong dependence on ξ, $\tau \propto \xi^4$, shows that very smooth distortions (large ξ) may not be sufficient for spatial inhomogeneity of phase-separating NOA65.

Regular morphologies. Regularly distorted director patterns can be used to fabricate regular polymer architectures, as we show below for the "fingerprint" cholesteric textures in cells with homeotropic alignment (lecithin coatings). The cholesteric LC (pitch $p = 10\mu$m) was obtained by adding a chiral agent CB15 (EM Industries) to E7/NOA65 mixture. The E7/CB15/NOA65 mixture was doped with a fluorescent dye acridine orange base (0.1 wt %) for confocal polarizing microscope (Olympus Fluoview BX-50) observations. Confocal microscopy allows one to obtain thin (micron scale) optical slices of the sample both in the horizontal and vertical planes, see, e.g., Refs. [4,9,11,24].

Before phase separation, the dye is distributed homogeneously [21], and the confocal polarizing microscope images the director field, since the anisometric dye molecules are oriented by $\hat{\mathbf{n}}$. Different orientations result in different intensity of fluorescence [24]: minimum

when $\hat{\mathbf{n}}$ is along the z-axis and maximum when $\hat{\mathbf{n}}$ is parallel to the polarization of the probing light. The vertical (xz) cross-section has a characteristic diamond-like shape, with the axis slightly tilted away from the z-axis, Fig. 4a. The confocal image corresponds to the computer-simulated equilibrium director $\hat{\mathbf{n}}(x,z)$, Fig. 4b. With the known $\hat{\mathbf{n}}(x,z)$, one can map the local energy density $f(x,z)$, Eq. (1) with the added twist term $2\pi K_2\left(\hat{\mathbf{n}}\cdot curl\hat{\mathbf{n}}\right)/p$. The energy pattern, Fig. 4c, shows that subsurface regions are distorted stronger than the bulk of the cell. It is easy to understand, since in the bulk, $\hat{\mathbf{n}}$ has a favorable helical structure, whereas near the boundaries, energetically costly bend and splay occur to satisfy the perpendicular boundary condition.

The morphology of phase-separation induced by nonpolarized UV-light is modulated in accordance with the fingerprint structure. In the phase separated system, the acridine dye tends to accumulate in the polymer component rather than in the LC [25]. In the confocal textures, Figs. 4d,e, the stained NOA65-rich particles appear bright on the dark LC background. Comparison of thin horizontal (x,y) optical slices near the bounding plates reveals that the particles are located exactly in the places with the maximum energy of director distortions, Fig. 4c-e (these confocal microscopy data are also confirmed by our scanning-electron microscopy observations). Light polarization mechanism also helps to accumulate NOA65 in these places, even when light is not polarized, since $n_z < 1$.

Summary. The director field can influence the pattern of phase separation from the LC solvent: the regions with the strongest director distortions can attract the phase-separating component. The effect demonstrates a principal difference between phase separation in isotropic and ordered anisotropic solvents. Similar effect might be expected even when the initial state of an anisotropic solvent is uniform: phase-separating particles that reach a characteristic size L_p will distort the director field and thus influence the phase separation around them. Further studies are needed to elucidate how the morphologies will be altered by such factors as the nature of monomer (e.g., mesogenic vs. non-mesogenic), diffusivity, reactivity, etc. We also demonstrated that the rate of NOA65 photopolymerization in a nematic LC is higher when the polarization of UV light is parallel to the director.

We thank L.-C. Chien, P. Palffy-Muhoray, S. Sprunt, J.L. West and D.-K. Yang for usefull discussions. The work has been supported by the NSF ALCOM grant, DMR 89-20147 and by donors of the Petroleum Research Fund, administered by ACS, grant 35306-AC7.

REFERENCES

[1] *Liquid crystals in complex geometries*, edited by G. P. Crawford and S. Zumer (Taylor & Francis, London, 1996).

[2] I. Dierking, L. L. Kosbar, A. Afzali-Ardakani, A. C. Lowe, and G. A. Held, Appl. Phys. Lett. **71**, 2454 (1997).

[3] R. A. M. Hikmet and H. Kemperman, Nature **392**, 476 (1998).

[4] K. Amundson, A. van Blaaderen, and P. Wiltzius, Phys. Rev. E **55**, 1646 (1997).

[5] T.J. Bunning, L.V. Natarajan, V.P. Tondiglia, and R.L. Sutherland, Annu. Rev. Mater. Sci. **30**, 83 (2000).

[6] Y. Kim, J. Francl, B. Taheri, J. L. West, Appl. Phys. Lett. **72**, 2253 (1998).

[7] A. M. Lapena, S. C. Glotzer, S. A. Langer, A.J. Liu, Phys. Rev. E **60**, 29 (1999).

[8] V. Vorflusev and S. Kumar, Science **283**, 1903 (1999).

[9] J. B. Nephew, T. C. Nihei, and S. A. Carter, Phys. Rev. Lett. **80**, 3276 (1998).

[10] J.-C. Loudet, P. Barois and P. Poulin, Nature **407**, 611 (2000).

[11] G. A. Held, L. L. Kosbar, I. Dierking, A. C. Lowe, G. Grinstein, V. Lee, and R.D. Miller, Phys. Rev. Lett. **79**, 3443 (1997).

[12] D. Voloschenko and O. D. Lavrentovich, J. Appl. Phys. **86**, 4843 (1999).

[13] S. W. Kang, S. Sprunt, L.-C. Chien, Appl. Phys. Lett. **76**, 3516 (2000).

[14] Technical Data Sheet for NOA65 Optical Adhesive, Norland Products, Inc., New Brunswick, NJ.

[15] G. W. Smith, Phys. Rev. Lett. **70**, 198 (1993).

[16] A. J. Lovinger, K. R. Amundson, and D. D. Davis, Chem. Mat. **6**, 1726 (1994).

[17] R. Bhargava, S.-Q. Wang, and J. L. Koenig, Macromolecules **32**, 8982 and 8989 (1999).

[18] D. Nwabunma, K. J. Kim, Yu. Lin, L.-C. Chien, Th. Kyu, Macromolecules **31**, 6806 (1998).

[19] L. Kielhorn and M. Muthukumar, J. Chem. Phys. **111**, 2259 (1999).

[20] J. A. Geurst, A. M. J. Spruijt, and C.J. Gerritsma, J. Phys. (France) **36**, 653 (1975).

[21] Before phase separation, a concentration inhomogeneity could decrease the macroscopic elastic energy through concentration dependence of elastic constants. However, the entropy term strongly opposes such inhomogeneity, so the relative variation in concentration does not exceed 10^{-4} [S. V. Shiyanovskii and J. G. Terentieva, Phys. Rev E **49**, 916 (1994)].

[22] P. Poulin and D. A. Weitz, Phys. Rev. E **57**, 626 (1998); M. Zapotocky, L. Ramos, P. Poulin, T.C. Lubensky, D.A.Weitz, Science **283**, 209 (1999).

[23] O. V. Kuksenok, R. W. Ruhwandl, S. V. Shiyanovskii, E. M.Terentjev, Phys. Rev. E **54**, 5198 (1996).

[24] I. I. Smalyukh, S. V. Shiyanovskii, and O. D. Lavrentovich, Chem. Phys. Lett. **336**, 88 (2001).

[25] S. Tahara, S. Niiyama, H. Kumai, T. Wakabayashi, Proc. SPIE **3297**, 44 (1998).

Figure Captions

FIG. 1. Polymerization dynamics in E7/NOA65. Microphotographs are taken after 35 min of UV exposure with (a) $\mathbf{P}\perp\hat{\mathbf{n}}$ and (b) $\mathbf{P}\|\hat{\mathbf{n}}$. Bright spots represent NOA65-rich

particles. (c) S/S_0 vs irradiation time for $\mathbf{P}\perp\hat{\mathbf{n}}$ (triangles) and $\mathbf{P}\|\hat{\mathbf{n}}$ (circles); S is the area occupied by precipitated particles, as seen under the microscope, S_0 is the whole area of CCD frame.

FIG. 2. UV photopolymerization near the (horizontal) defect boundary separating two twist domains in E7/NOA65. Two NOA65 particles marked by a circle and a square migrate to the boundary. Double arrow shows the directions of both $\mathbf{P}$ and $\hat{\mathbf{n}}$ at the cell plate facing the UV lamp. Time bars show the UV exposure time. Polarizing microscopy with uncrossed polarizers.

FIG. 3. Phase-separated E7/NOA65 near a defect boundary between two twist domains. Exposure time 1 hr. Uncrossed polarizers.

FIG.4. Phase separation in a homeotropic cell ($d = 10\ \mu m$) with cholesteric "fingerprints". (a), (b), (c) are the vertical cross sections of the cell, and (d) and (e) are the horizontal one. (a) confocal texture of $\hat{\mathbf{n}}(x,z)$; (b) computer simulated $\hat{\mathbf{n}}(x,z)$; $K_1 = 6.4$, K_2= 3, K_3= 10 (all in pN), $W_c d/K$= 10; W_c is the anchoring coefficient at the plates; (c) map of $f(x,z)$, higher energy densities are darker. Confocal textures of polymer particles near the upper plate (d) and the lower plate (e).

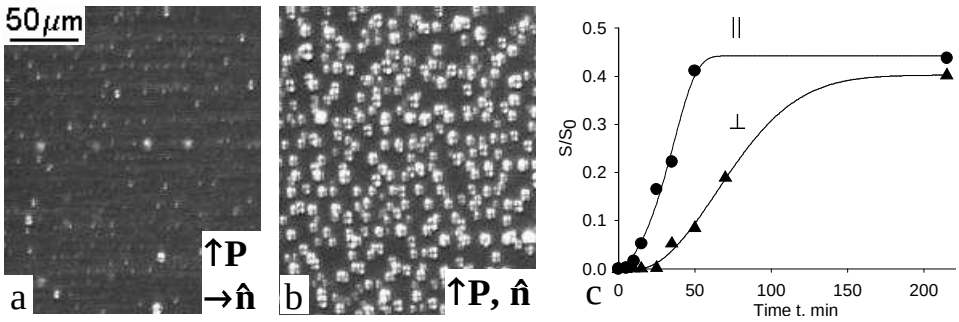
50 μm
↑P
→n̂
a
b
↑P, n̂
0.5
0.4
0.3
0.2
0.1
0.0
S/S0
||
⊥
0
50
100
150
200
Time t, min
c

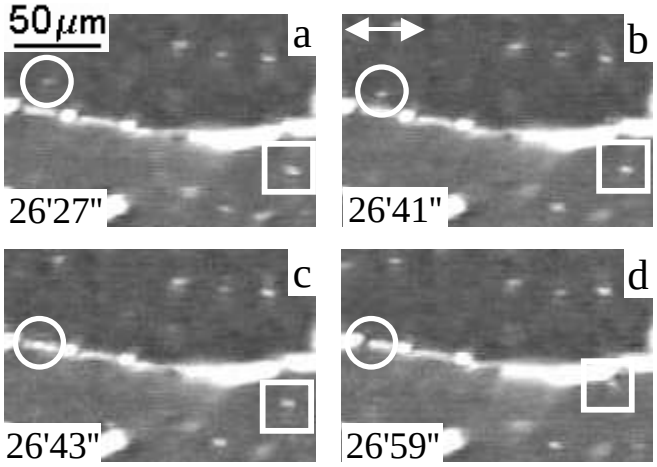
50 μm
a
26'27"
b
26'41"
c
26'43"
d
26'59"

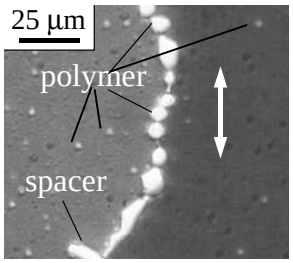
25 μm
polymer
spacer

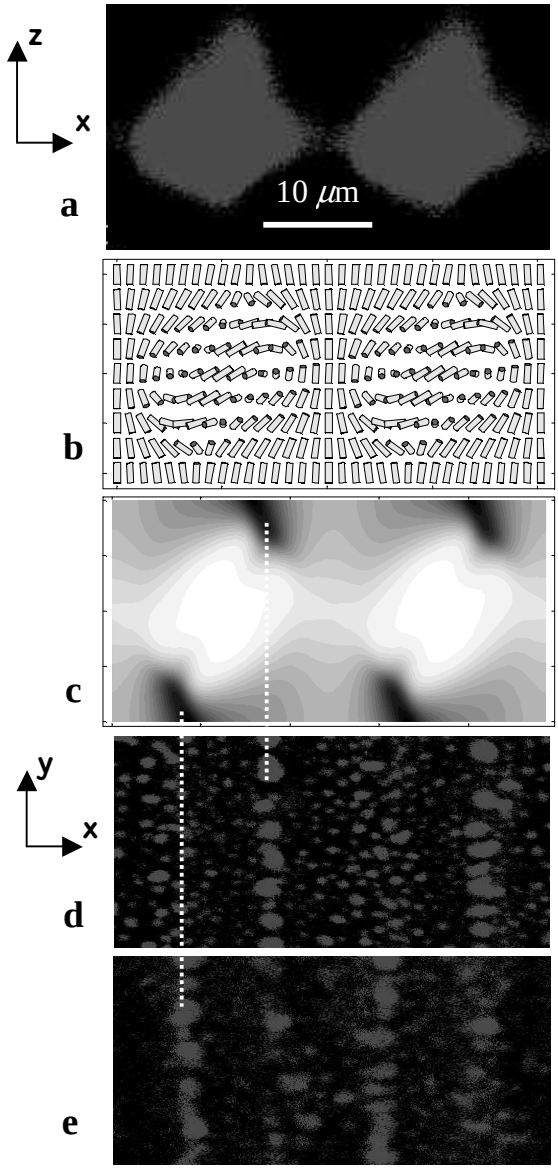
z
x
a
10 μm
b
c
y
x
d
e